

Commun. Theor. Phys. **76** (2024) 015103 (13pp) https://doi.org/10.1088/1572-9494/ad1325

Quantum gate-assisted teleportation in noisy environments: robustness and fidelity improvement

Sajede Harraz*, Jiaoyang Zhang and Shuang Cong*

Department of Automation, University of Science and Technology of China, Hefei 230027, China

E-mail: sajede@ustc.edu.cn and scong@ustc.edu.cn

Received 11 September 2023, revised 17 November 2023
Accepted for publication 7 December 2023
Published 19 January 2024

Abstract

Quantum teleportation as the key strategy for quantum communication requires pure maximally shared entangled states among quantum nodes. In practice, quantum decoherence drastically degrades the shared entanglement during entanglement distribution, which is a serious challenge for the development of quantum networks. However, most of the decoherence control strategies proposed thus far are either resource-intensive or time-consuming. To overcome this obstacle, we enable noise-resistant teleportation through a noisy channel with a limited number of qubits and without applying time-consuming weak measurements. We apply a quantum gate control unit consisting of a controlled NOT gate and a rotation gate after the original teleportation protocol is accomplished. Furthermore, we demonstrate that a teleportation fidelity of unity is attainable when environment-assisted measurement is added to the proposed teleportation protocol via quantum gates. Moreover, we present an entanglement distribution process by employing the designed quantum gate control unit followed by the deterministic standard teleportation protocol to improve teleportation fidelity by establishing improved shared entanglement. Our performance analysis indicates that the proposed teleportation schemes offer a competitive fidelity and success probability compared with the conventional schemes and a recent weak measurement-based teleportation protocol.

Keywords: quantum communication, quantum teleportation, decoherence control, quantum gate, environment-assisted measurement

(Some figures may appear in colour only in the online journal)

Abbreviations

ADC	Amplitude damping channel
EAM	Environment-assisted measurement
MQGTP	Maximized quantum gate-assisted teleportation protocol
MR	Quantum measurement and reversing operation
QGCU	Quantum gate control unit
QGED	Quantum gate-assisted entanglement distribution
QGTP	Quantum gate-assisted teleportation protocol
QGTP-EAM	Quantum gate-assisted teleportation protocol combined with environment-sssisted measurement
STNP	Standard teleportation with no protection

1. Introduction

Quantum communication, an indispensable branch of quantum information, mainly involves quantum teleportation [1–5], quantum dense coding [6–8], quantum secret sharing [9–11] and quantum key distribution [12–14]. Quantum communication, leveraging the intrinsic characteristics of quantum mechanics,

* Authors to whom any correspondence should be addressed.

offers a significantly higher level of security than classical communication [15]. Quantum teleportation is the key strategy for transmitting quantum information without physically transferring the particle that contains the quantum information [16]. Scalable quantum networks depend greatly on quantum teleportation, which has attracted special attention and has made considerable breakthroughs both theoretically and experimentally (see, for example, [16–19] and references therein). Additionally, distributed quantum computing is established by using quantum teleportation circuits to transfer quantum information between distant quantum processors within a quantum network [20].

It is theoretically proven that in an ideal noiseless environment the state of an arbitrary unknown qubit can be 'reproduced' in another location with both average fidelity and success probability equal to one by implementing specific quantum teleportation protocols such as the protocols proposed in [21–23]. However, in practical quantum information processing tasks, decoherence occurs due to the inevitable interaction of the quantum system with the environment [24, 25]; this is one of the major obstacles to establishing a quantum network or connecting components in a scalable quantum architecture. Likewise, decoherence of shared entanglement caused by environmental noise is an important source of imperfections in quantum teleportation [26, 27]. Amplitude damping is one of the most important decoherence mechanisms; it describes the energy dissipation of a quantum system and is a major cause of imperfections in practical quantum communication in quantum networks and quantum computing [28–31]. To improve the performance of quantum teleportation in the presence of noise, two interesting decoherence suppression schemes—weak measurement and quantum measurement reversal [32–34] and quantum feed-forward control and its reversal [35, 36]—have been applied to the protection of shared entanglement. In fact, these schemes follow a similar strategy, namely the application of control operations both before and after the noisy channel. Before the noisy channel, the state of the system is transferred to a state that is less vulnerable to the effects of the noise, and after the noisy channel reversal operations are applied to restore the system to its initial state. In addition, environment-assisted measurement (EAM) is a powerful technique to overcome the effects of the decoherence channel [37–40, 53]. This technique performs a measurement on the noisy channel to select the system states that correspond to the desired measurement outcome of the environment; therefore, restoration operations are applied on the system conditioned on the results of the measurement on the environment. Moreover, quantum error correction shows bright prospects for application in enhancing quantum entanglement [26, 41], although it requires redundant qubits in entanglement. In all the above schemes the focus is on the entanglement distribution process, while it has been shown that the effects of the decoherence channel can be effectively suppressed by modifying the quantum teleportation protocol itself [42–44]. In [43, 44], a generalized concept of quantum teleportation in the framework of a quantum measurement and reversing operation (MR) was introduced, where the joint Bell state measurement and a corresponding single-qubit reversal operation were suggested. In the MR framework, a well-designed weak measurement operator takes the place of standard unitary operators in the final step of the original quantum teleportation protocol. However, utilizing time-consuming weak measurements (such as monitoring cavities by photon counting devices) slows the whole teleportation process. In fact, the rapidity of quantum teleportation is of vital significance and a necessity for advanced quantum networks and quantum computing. Hence, how to develop a more rapid protection scheme suitable for quantum teleportation protocols remains an open question. Zubairy's group [45–47] has shown that quantum gates can replace weak measurements in retrieving quantum states and protecting entanglement. They applied a Hadamard gate on an ancilla qubit and subsequently a controlled NOT (CNOT) gate on the combined system consisting of the system qubit and the ancilla qubit to entirely reverse the effect of weak measurement. One of the most significant advantages of the quantum state protection scheme via quantum gates is that it can be implemented in a shorter time than weak measurement reversal. Hence, it is more suitable for quantum networks and quantum computing.

In this paper, we utilize quantum gates to enable noise-resistant quantum teleportation through noisy channels. Unlike previous decoherence control strategies, our proposed schemes neither require redundant qubits in entanglement nor employ time-consuming weak measurements. We apply a quantum gate control unit (QGCU) in the last step of teleportation after the completion of the standard teleportation procedure. Specifically, we apply an appropriate rotation transformation to an ancilla qubit prepared in the ground state, interact the ancilla qubit with the receiver qubit and then apply a CNOT gate on the combined system. The proposed quantum gate-assisted teleportation protocol (QGTP) is considered to be successful if the ancilla qubit is measured in a certain state. To further improve the fidelity of teleportation, we demonstrate that it is possible to achieve unit average teleportation fidelity independent of the degree of decoherence and the input state parameters by applying EAM in the entanglement distribution process and a QGCU at the location of the receiver, and deduce the specific formula of the optimum rotation gate angle to gain unit average teleportation fidelity. Since the proposed teleportation protocols via QGCU are probabilistic, we also consider applying QGCU only in the entanglement distribution process followed by a deterministic standard teleportation protocol. The proposed entanglement distribution process aims to transfer the shared entanglement to a state that is robust to decoherence via a QGCU before the noisy channel, and recover the shared entanglement via another QGCU after the noisy channel. We should point out that the noisy channel is assumed to be fully characterized, i.e. the magnitude of decoherence is known and quantum gates can be implemented perfectly, hence the fault of quantum gates is not taken into account [48–50]. For comparison, we study standard teleportation with no protection (STNP) and teleportation in the MR framework, and show the improvement of the average teleportation fidelity of our proposed teleportation schemes by numerical simulations.

The remainder of this paper is organized as follows. In section 2, we present the proposed teleportation protocols via quantum gates and EAM through a noisy channel, and analyze their performance in detail. In section 3, we investigate the entanglement distribution via quantum gates, where we apply a QGCU before the noisy channel at the sender's

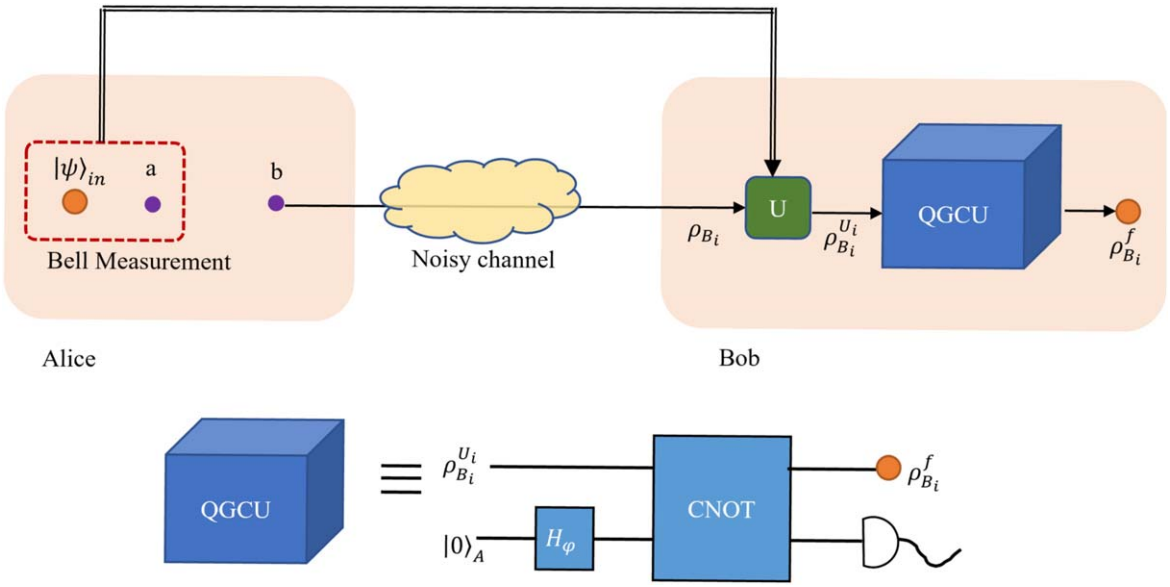

Figure 1. Schematic diagram of the QGTP. The double lines indicate the classical communications.

location and another QGCU after the noisy channel at the receiver's location. Finally, our conclusion is drawn in section 4.

2. Teleportation protocols through an amplitude damping channel via quantum gates

In this section we give details of the two proposed QGTPs through an amplitude damping channel (ADC). We consider the scenario in which Alice prepares the maximally shared entangled state and then distributes one particle to Bob through an ADC. In the first protocol, we only employ the designed QGCU in the last step of teleportation to overcome the effects of the ADC and retrieve the input state at Bob's location. In the second protocol, to further improve the teleportation fidelity, we combine the EAM technique in the entanglement distribution process with the first proposed protocol. Afterwards, we compare the average teleportation fidelity and the total teleportation success probability of the two proposed QGTPs.

2.1. Quantum gate-assisted teleportation protocol through ADC

In this subsection, we suggest a QGTP to achieve high-fidelity quantum teleportation through an ADC, where the receiver applies a QGCU to his qubit after the standard teleportation protocol is accomplished. First, let us calculate the output state of the standard teleportation protocol through the ADC before the QGCU is employed.

The input state that Alice wishes to teleport to Bob is presented as

$$\rho_{\rm in} = |\psi_{\rm in}\rangle\langle\psi_{\rm in}| = \begin{bmatrix} |\alpha|^2 & \alpha\beta^* \\ \alpha^*\beta & |\beta|^2 \end{bmatrix}, \tag{1}$$

where $|\alpha|^2 + |\beta|^2 = 1$ and $*$ denotes complex conjugation.

The maximally entangled state prepared by Alice is defined as

$$|\psi\rangle_{ab} = \frac{1}{\sqrt{2}}(|0\rangle_a|0\rangle_b + |1\rangle_a|1\rangle_b), \tag{2}$$

where she keeps the first qubit and sends the second qubit of the entangled pair to Bob through a noisy channel. In this paper, we consider the ADC, which is described by the well-known Kraus operators, as [15]

$$e_0 = \begin{bmatrix} 1 & 0 \\ 0 & \sqrt{1-r} \end{bmatrix}, \; e_1 = \begin{bmatrix} 0 & \sqrt{r} \\ 0 & 0 \end{bmatrix}, \tag{3}$$

where $0 \leqslant r \leqslant 1$ is the magnitude of the decoherence and represents the probability of decay from the upper level $|1\rangle$ to the lower level $|0\rangle$ with $r = 1 - {\rm e}^{-\Gamma t}$, in which Γ is the energy relaxation rate and t is the evolving time.

By following the standard teleportation protocol, Bob's non-normalized states, corresponding to Alice's different joint Bell state measurement results, are described as

$$\rho_{B_i}^{U_i}(i = 1, 2) = \frac{1}{4}\begin{bmatrix} |\alpha|^2 + |\beta|^2 r & \alpha\beta^*\sqrt{1-r} \\ \alpha^*\beta\sqrt{1-r} & |\beta|^2(1-r) \end{bmatrix},$$
$$\rho_{B_i}^{U_i}(i = 3, 4) = \frac{1}{4}\begin{bmatrix} |\alpha|^2(1-r) & \alpha\beta^*\sqrt{1-r} \\ \alpha^*\beta\sqrt{1-r} & |\beta|^2 + |\alpha|^2 r \end{bmatrix}. \tag{4}$$

The detailed procedure of the standard teleportation protocol is presented in the appendix.

According to equation (4), Bob's output state is severely damped due to the effects of the ADC, which causes a significant decrease in teleportation fidelity. In the following, we employ the QGCU in the last step of teleportation to compensate for the effects of the ADC and retrieve the input state at Bob's end. After finishing the standard teleportation process, Bob performs the following operations based on

quantum gates on his damped output qubit in equation (4). Hereafter, we refer to these operations realized by quantum gates as the QGCU. A schematic diagram of our proposed QGTP is shown in figure 1.

Apart from a CNOT and a rotation gate, the QGCU also contains an ancilla qubit in the state $|0\rangle$, for example an atom in the ground state that can interact with the cavity field [45]. A rotation gate $H_\varphi = [\cos\varphi, -\sin\varphi; \sin\varphi, \cos\varphi]$ with an angle φ is applied on the ancilla qubit. Hence, the state of the ancilla qubit after passing through the rotation gate is

$$\rho_A = \begin{bmatrix} \cos^2\varphi & \cos\varphi\sin\varphi \\ \cos\varphi\sin\varphi & \sin^2\varphi \end{bmatrix}. \tag{5}$$

Bob's combined state after he interacts the ancilla qubit with the damped state in equation (4) is given as

$$\rho_{B_i}^{A} = \rho_{B_i}^{U_i} \otimes \rho_A. \tag{6}$$

Afterwards, a CNOT gate is applied on the pair comprising Bob's qubit and the ancilla qubit, where Bob's qubit is the controlled qubit and the ancilla qubit is the target qubit. The CNOT gate is defined as

$$C = \begin{bmatrix} 1 & 0 & 0 & 0 \\ 0 & 1 & 0 & 0 \\ 0 & 0 & 0 & 1 \\ 0 & 0 & 1 & 0 \end{bmatrix}. \tag{7}$$

The state of the whole system after applying the CNOT gate can be described in the systematic basis ($|00\rangle$, $|01\rangle$, $|10\rangle$ and $|11\rangle$) by

$$\begin{aligned} \rho_{B_i}^{C} &= C\rho_{B_i}^{A}C^{\dagger} \\ &= \cos^2\varphi \begin{bmatrix} \rho_{B_i}^{U_i}(1,1) & \rho_{B_i}^{U_i}(1,1)\tan\varphi & \rho_{B_i}^{U_i}(1,2)\tan\varphi & \rho_{B_i}^{U_i}(1,2) \\ \rho_{B_i}^{U_i}(1,1)\tan\varphi & \rho_{B_i}^{U_i}(1,1)\tan^2\varphi & \rho_{B_i}^{U_i}(1,2)\tan^2\varphi & \rho_{B_i}^{U_i}(1,2)\tan\varphi \\ \rho_{B_i}^{U_i}(2,1)\tan\varphi & \rho_{B_i}^{U_i}(2,1)\tan^2\varphi & \rho_{B_i}^{U_i}(2,2)\tan^2\varphi & \rho_{B_i}^{U_i}(2,2)\tan\varphi \\ \rho_{B_i}^{U_i}(2,1) & \rho_{B_i}^{U_i}(2,1)\tan\varphi & \rho_{B_i}^{U_i}(2,2)\tan\varphi & \rho_{B_i}^{U_i}(2,2) \end{bmatrix}. \end{aligned} \tag{8}$$

At this point, a projective measurement is made on the state of the ancilla qubit dependent on Alice's joint Bell state measurement result. Hence, the success of a QGCU as the final step of teleportation depends on a particular outcome in the measurement of the ancilla qubit. When the measurement results correspond to $B_{1,2}$ ($B_{3,4}$) as specified in equation (A4), the teleportation is considered successful if the measurement result of the ancilla qubit is $|0\rangle$ ($|1\rangle$). Hence, the state of the whole system is described as

$$\rho_{B_i}^{C'} = P_{B_i}^{A}\rho_{B_i}^{C}P_{B_i}^{A\dagger}, \tag{9}$$

where $P_{B_{1,2}}^{A} = I_2 \otimes |0\rangle\langle 0|$ and $P_{B_{3,4}}^{A} = I_2 \otimes |1\rangle\langle 1|$ are the projection operators corresponding to Alice's different measurement results with I_2 being the 2×2 identity operator.

Finally, Bob's reduced density matrix is calculated by tracing out the ancilla qubit as

$$\begin{aligned} \rho_{B_i}^{f}(i=1,2) &= \frac{\mathrm{Tr}_A(\rho_{B_i}^{C'})}{\mathrm{Tr}\left[\mathrm{Tr}_A(\rho_{B_i}^{C'})\right]} \\ &= \frac{1}{\rho_{B_i}^{U_i}(1,1) + \rho_{B_i}^{U_i}(2,2)\tan^2\varphi} \\ &\quad \begin{bmatrix} \rho_{B_i}^{U_i}(1,1) & \rho_{B_i}^{U_i}(1,2)\tan\varphi \\ \rho_{B_i}^{U_i}(2,1)\tan\varphi & \rho_{B_i}^{U_i}(2,2)\tan^2\varphi \end{bmatrix}, \\ \rho_{B_i}^{f}(i=3,4) &= \frac{\mathrm{Tr}_A(\rho_{B_i}^{C'})}{\mathrm{Tr}\left[\mathrm{Tr}_A(\rho_{B_i}^{C'})\right]} \\ &= \frac{1}{\rho_{B_i}^{U_i}(1,1)\tan^2\varphi + \rho_{B_i}^{U_i}(2,2)} \\ &\quad \begin{bmatrix} \rho_{B_i}^{U_i}(1,1)\tan^2\varphi & \rho_{B_i}^{U_i}(1,2)\tan\varphi \\ \rho_{B_i}^{U_i}(2,1)\tan\varphi & \rho_{B_i}^{U_i}(2,2) \end{bmatrix}. \end{aligned} \tag{10}$$

Furthermore, the success probability of gaining the state $\rho_{B_i}^{f}$ is calculated as

$$\begin{aligned} g_{B_i}^{f}(i=1,2) &= \mathrm{Tr}\left[\mathrm{Tr}_A(\rho_{B_i}^{C'})\right] \\ &= \frac{1}{4}\cos^2\varphi(|\alpha|^2 + |\beta|^2 r + |\beta|^2(1-r)\tan^2\varphi), \\ g_{B_i}^{f}(i=3,4) &= \mathrm{Tr}\left[\mathrm{Tr}_A(\rho_{B_i}^{C'})\right] \\ &= \frac{1}{4}\cos^2\varphi(|\beta|^2 + |\alpha|^2 r + |\alpha|^2(1-r)\tan^2\varphi), \end{aligned} \tag{11}$$

where $\mathrm{Tr}_A(\bullet)$ is the partial trace over the ancilla qubit.

To evaluate the performance of the proposed QGTP, we consider the fidelity between the input state in equation (1) and the final state received by Bob in equation (10) as

$$\begin{aligned} \mathrm{fid}_i(i=1,2) &= \langle\psi_{\mathrm{in}}|\rho_{B_i}^{f}|\psi_{\mathrm{in}}\rangle \\ &= \frac{|\alpha|^4 + |\alpha|^2|\beta|^2 r + 2|\alpha|^2|\beta|^2\sqrt{1-r}\tan\varphi + |\beta|^4\tan^2\varphi(1-r)}{|\alpha|^2 + |\beta|^2 r + |\beta|^2(1-r)\tan^2\varphi}, \\ \mathrm{fid}_i(i=3,4) &= \langle\psi_{\mathrm{in}}|\rho_{B_i}^{f}|\psi_{\mathrm{in}}\rangle \\ &= \frac{|\beta|^4 + |\alpha|^2|\beta|^2 r + 2|\alpha|^2|\beta|^2\sqrt{1-r}\tan\varphi + |\alpha|^4\tan^2\varphi(1-r)}{|\beta|^2 + |\alpha|^2 r + |\alpha|^2(1-r)\tan^2\varphi}. \end{aligned} \tag{12}$$

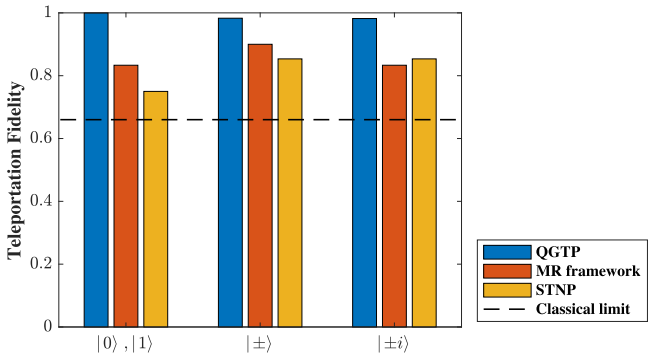

Figure 2. Total teleportation fidelity for specific input states. The dashed black line indicates the classical limit of $2/3$. Here $r = 0.5$.

It can be seen for equation (12) that a rotation gate angle φ such that the teleportation fidelity is always equal to one for all values of r in QGTP does not exist for all input states; nevertheless, for some specific input states, for example $|0\rangle$ and $|1\rangle$, a teleportation fidelity equal to one is achievable regardless of the value of φ and r.

Accordingly, by considering the probability of gaining different measurement results from Alice in equation (A6) and the corresponding fidelities in equation (12), the total teleportation fidelity of the proposed QGTP is described as

$$\mathrm{fid}_{\mathrm{tot}}^{\mathrm{QGTP}} = \sum_{i=1,2,3,4} (P_{B_i}\mathrm{fid}_i) = \frac{1}{4}(\mathrm{fid}_1 + \mathrm{fid}_2 + \mathrm{fid}_3 + \mathrm{fid}_4). \tag{13}$$

According to equations (12) and (13), the total teleportation fidelity is dependent on the input state ρ_{in} parameters. Thus, to assess the performance of the proposed QGTP in a way that is independent of a certain input state, we utilize the average teleportation fidelity over all possible input states as

$$\begin{aligned}\mathrm{Fid}_{\mathrm{av}}^{\mathrm{QGTP}} &= \int \mathrm{d}\rho \mathrm{fid}_{\mathrm{tot}}^{\mathrm{QGTP}} \\ &= \int \mathrm{d}\rho \frac{1}{4}(\mathrm{fid}_1 + \mathrm{fid}_2 + \mathrm{fid}_3 + \mathrm{fid}_4).\end{aligned} \tag{14}$$

Moreover, the total teleportation success probability of the proposed QGTP is calculated as

$$\begin{aligned}g_{\mathrm{tot}}^{\mathrm{QGTP}} &= \sum_{i=1,2,3,4} g_{B_i}^{f} \\ &= \frac{1}{2}\cos^2\varphi(1 + r + (1 - r)\tan^2\varphi),\end{aligned} \tag{15}$$

where $g_{B_i}^{f}$ is the success probability of gaining the state $\rho_{B_i}^{f}$ defined in equation (11).

For comparison, we consider STNP through an ADC. The total teleportation fidelity between the input state equation (1) and the final state received by Bob in equation (4) is

$$\begin{aligned}\mathrm{fid}_{\mathrm{tot}}^{\mathrm{STNP}} &= \frac{1}{2}[(|\alpha|^4 + |\beta|^4)(2 - r) \\ &+ |\alpha|^2|\beta|^2(4\sqrt{1 - r} + 2r)].\end{aligned} \tag{16}$$

Therefore, the average teleportation fidelity of the STNP over all possible input states is presented as

$$\begin{aligned}\mathrm{Fid}_{\mathrm{av}}^{\mathrm{SNTP}} &= \int \mathrm{d}\rho \left\{ \frac{1}{2}[(|\alpha|^4 + |\beta|^4)(2 - r) \right. \\ &\left. + |\alpha|^2|\beta|^2(4\sqrt{1 - r} + 2r)] \right\} \\ &= \frac{1}{15}(4\sqrt{1 - r} - \frac{7}{2}r + 11).\end{aligned} \tag{17}$$

For further comparison, we also consider another probabilistic teleportation protocol that is based on weak measurement, i.e. the MR framework of teleportation [43]. In the MR framework, Bob applies designed weak measurement reversal instead of unitary operations to suppress the effects of the ADC. By considering the maximally shared entangled state in equation (2), the total teleportation fidelity of the MR framework is presented as

$$\mathrm{fid}_{\mathrm{tot}}^{\mathrm{MR}} = \frac{1}{2}\left(\frac{1 + r|\alpha|^2|\beta|^2}{1 + r|\beta|^2} + \frac{1 + r|\alpha|^2|\beta|^2}{1 + r|\alpha|^2}\right). \tag{18}$$

Consequently, the average teleportation fidelity of the MR framework over all possible input states is described as

$$\mathrm{Fid}_{\mathrm{av}}^{\mathrm{MR}} = \int d\rho \left[\frac{1}{2}\left(\frac{1 + r|\alpha|^2|\beta|^2}{1 + r|\beta|^2} + \frac{1 + r|\alpha|^2|\beta|^2}{1 + r|\alpha|^2}\right)\right]. \tag{19}$$

The MR framework of teleportation is probabilistic due to the incompleteness of the weak measurement reversal employed in the last step of the teleportation procedure. The total teleportation success probability of the MR framework is defined as

$$g_{\mathrm{tot}}^{\mathrm{MR}} = \frac{2 - r - r^2}{2}. \tag{20}$$

In figure 2, we compare the total teleportation fidelity of our proposed QGTP with the MR framework and STNP for various input states in the presence of amplitude damping noise. In particular, we calculate the total teleportation fidelity by selecting specific input states in mutually unbiased bases on the Bloch sphere, i.e. $|0\rangle$, $|1\rangle$, $|\pm\rangle = (|0\rangle \pm |1\rangle)/\sqrt{2}$ and $|\pm i\rangle = (|0\rangle \pm i|1\rangle)/\sqrt{2}$ [51].

Figure 2 shows that the proposed QGTP outperforms the MR framework and STNP with a total teleportation fidelity of more than 0.98 for various selected input states. Additionally, it can be seen that when the input state is $|0\rangle$ or $|1\rangle$, the effects of the ADC can be totally canceled and the unit teleportation fidelity is attainable by applying the optimum rotation gate angle φ.

Note here that while the total teleportation fidelity is reliant on the input state parameters, the average teleportation fidelity considers all possible input states and is independent of the input state parameters. From now on, we use the average teleportation fidelity as the performance indicator to evaluate the behavior of teleportation protocols.

In figure 3(a), we depict the average teleportation fidelity of the QGTP in equation (14), the average teleportation fidelity of the MR framework in equation (19) (the green

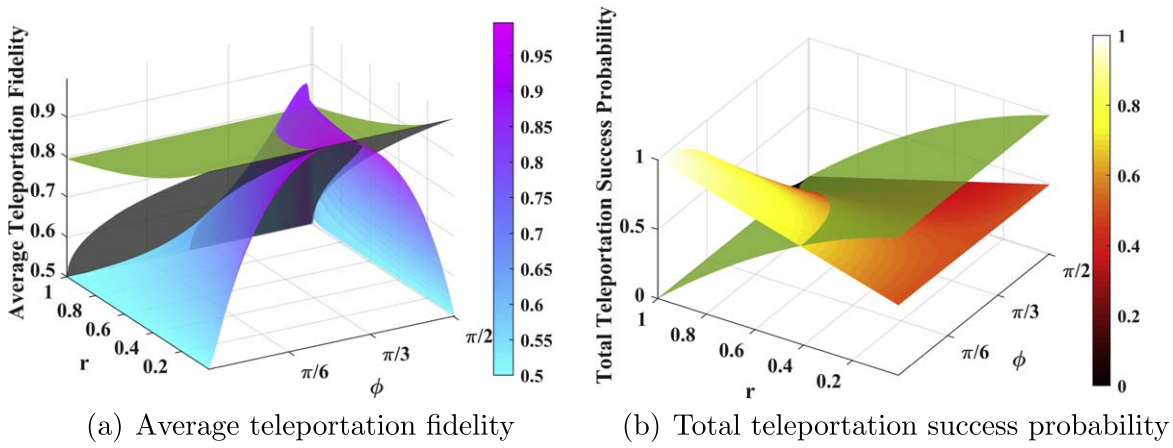

Figure 3. Average teleportation fidelity and total teleportation success probability as a function of the rotation gate angle φ and magnitude of the decoherence r. The planes with a color map indicate the proposed QGTP, the green planes correspond to the MR framework and the gray plane corresponds to STNP.

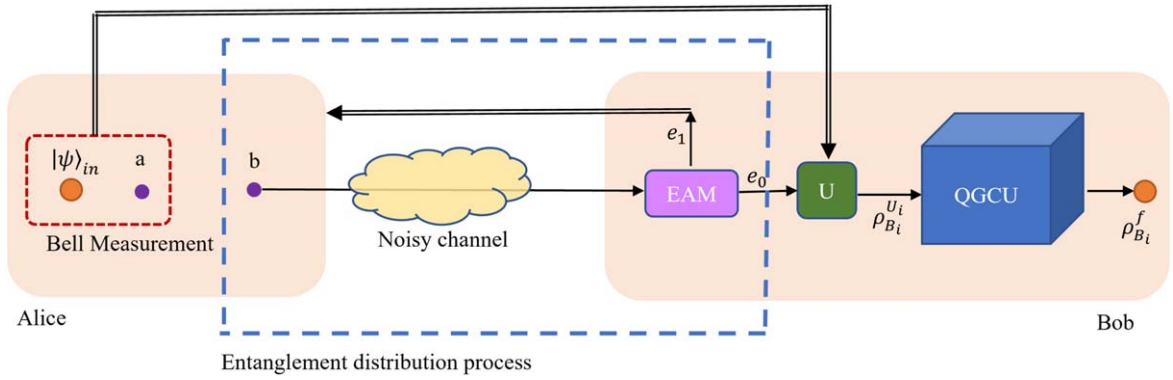

Figure 4. Schematic diagram of QGTP-EAM.

plane) and the average teleportation fidelity of STNP in equation (17) (the gray plane) as a function of the rotation gate angle φ and the magnitude of the decoherence r are presented. Moreover, figure 3(b) is the total teleportation success probability of the QGTP in equation (15) and the total teleportation success probability of the MR framework in equation (20) (the green plane) versus φ and r. We highlight that STNP is a deterministic protocol, meaning the teleportation success probability is always equal to one. Therefore, we have excluded the success probability of STNP in figure 3(b).

As figure 3(a) shows, for each r, the maximum teleportation fidelity of the QGTP is greater than that of the MR framework. Thus, by selecting the optimum rotation gate angle φ, the teleportation fidelity can be improved for each r compared with the MR framework. Additionally, as shown in figure 3(b), the total teleportation success probability of the QGTP is higher for smaller rotation gate angles and can be enhanced for intense r compared with that of the MR framework. However, for the optimum range of φ to maximize the average teleportation fidelity, the corresponding total teleportation success probability is lower than that of the MR framework. We shall discuss the maximized average teleportation fidelity and corresponding total teleportation success probability of the QGTP later in section 2.3.

2.2. Further improving the teleportation fidelity of QGTP via environment-assisted measurement

In this section, we add the EAM technique to the entanglement distribution process of the QGTP to further improve the teleportation fidelity. We emphasize once more that the noisy channel is assumed to be fully characterized, i.e. Bob knows the value of r, which cannot be obtained freely. A schematic diagram of the QGTP combined with EAM (QGTP-EAM) is presented in figure 4.

First, we give a brief explanation of the fundamental concept of EAM. The basic idea of EAM is to perform a measurement on the environment (decoherence channel) coupled to the system of interest; hence, the environment collapses to the eigenstates of the measured observable. As a result, the system will be projected into a state relative to each resulting environmental state. The aim is to keep the system states corresponding to invertible Kraus operators of the environment and discard other results [52, 53, 54]. To do so, a detector is added to monitor the excitation changes in the environment. If the measurement result is represented by 'no click', it means that the resulting environmental state is e_0, so we keep the corresponding system states and discard other measurement results since they are non-invertible.

The scenario is almost the same as that in section 2. Alice prepares the entangled state in equation (2) and sends one

qubit through an ADC to Bob. Then, Bob applies EAM to the ADC and tells the result to Alice. If the ADC is in an unexcited state related to the invertible Kraus operator e_0 in equation (3), entanglement distribution is successfully achieved, and the teleportation process can be started. Otherwise, he discards the entanglement distribution at this time and restarts the process. In other words, we only keep the damped entanglement corresponding to the invertible Kraus operator e_0. Hence, the shared entangled state after a successful EAM is described as

$$\rho_{ab}^{\mathrm{EAM}} = \frac{E_0\rho_{ab}E_0^{\dagger}}{g^{\mathrm{ED-EAM}}} = \frac{1}{2-r} \times \begin{bmatrix} 1 & 0 & 0 & \sqrt{1-r} \\ 0 & 0 & 0 & 0 \\ 0 & 0 & 0 & 0 \\ \sqrt{1-r} & 0 & 0 & 1-r \end{bmatrix}, \tag{21}$$

where $g^{\mathrm{ED-EAM}} = \mathrm{Tr}\,(E_0\rho_{ab}E_0^{\dagger}) = 1 - r/2$ is the success probability of the entanglement distribution via EAM.

After the entanglement distribution via EAM has been done successfully, Alice starts the teleportation process by interacting the input qubit with her half of the entangled shared state and applies the joint Bell state measurement with measurement operators given in equation (A4). The non-normalized state of Bob's qubit corresponding to Alice's different measurement results B_i $(i = 1, 2, 3, 4)$ after applying the unitary operations given in equation (A7) becomes

$$\rho_{\mathrm{EAM}_{B_i}}^{U_i}(i=1,2) = \frac{1}{4-2r} \times \begin{bmatrix} |\alpha|^2 & \alpha\beta^*\sqrt{1-r} \\ \alpha^*\beta\sqrt{1-r} & |\beta|^2(1-r) \end{bmatrix},$$
$$\rho_{\mathrm{EAM}_{B_i}}^{U_i}(i=3,4) = \frac{1}{4-2r} \times \begin{bmatrix} |\alpha|^2(1-r) & \alpha\beta^*\sqrt{1-r} \\ \alpha^*\beta\sqrt{1-r} & |\beta|^2 \end{bmatrix}. \tag{22}$$

Now, to recover the damped state in equation (22), Bob needs to apply the QGCU explained in section 2.2. Hence, Bob's final density matrix after applying the QGCU is described as

$$\rho_{\mathrm{EAM}_{B_i}}^{f}(i=1,2) = \frac{1}{|\alpha|^2 + |\beta|^2(1-r)\tan^2\varphi} \times \begin{bmatrix} |\alpha|^2 & \alpha\beta^*\sqrt{1-r}\tan\varphi \\ \alpha^*\beta\sqrt{1-r}\tan\varphi & |\beta|^2(1-r)\tan^2\varphi \end{bmatrix},$$
$$\rho_{\mathrm{EAM}_{B_i}}^{f}(i=3,4) = \frac{1}{|\alpha|^2(1-r)\tan^2\varphi + |\beta|^2} \times \begin{bmatrix} |\alpha|^2(1-r)\tan^2\varphi & \alpha\beta^*\sqrt{1-r}\tan\varphi \\ \alpha^*\beta\sqrt{1-r}\tan\varphi & |\beta|^2 \end{bmatrix}. \tag{23}$$

The success probability of gaining the state $\rho_{\mathrm{EAM}_{B_i}}^{f}$ is calculated as

$$g_{\mathrm{EAM}_{B_i}}^{f}(i=1,2) = \frac{1}{4-2r}\cos^2\varphi(|\alpha|^2 + |\beta|^2(1-r)\tan^2\varphi),$$
$$g_{\mathrm{EAM}_{B_i}}^{f}(i=3,4) = \frac{1}{4-2r}\cos^2\varphi(|\beta|^2 + |\alpha|^2(1-r)\tan^2\varphi). \tag{24}$$

To achieve unit teleportation fidelity, Bob's output state in equation (23) must be the same as the input state in equation (1); hence, the optimum rotation gate angle is determined as

$$\varphi_{\mathrm{opt}}^{\mathrm{QGTP-EAM}} = \tan^{-1}\left(\frac{1}{\sqrt{1-r}}\right). \tag{25}$$

By selecting the optimum rotation gate angle in equation (25) the teleportation fidelity is always equal to one, i.e. $\mathrm{fid}_{\mathrm{EAM}_{B_i}} = \langle\psi_{\mathrm{in}}|\rho_{\mathrm{EAM}_{B_i}}^{f}|\psi_{\mathrm{in}}\rangle = 1$. Consequently, the average teleportation fidelity of the proposed QGTP-EAM over all possible input states becomes

$$\mathrm{Fid}_{\mathrm{av}}^{\mathrm{QGTP-EAM}} = \int d\rho \sum_{i=1,2,3,4}(P_{\mathrm{EAM}_{B_i}}\mathrm{fid}_{\mathrm{EAM}_{B_i}}) = 1, \tag{26}$$

where $P_{\mathrm{EAM}_{B_i}}$ is the probability of gaining the measurement outcome corresponding to the measurement operator B_i in the QGTP-EAM as

$$P_{\mathrm{EAM}_{B_i}}(i=1,2) = \frac{|\alpha|^2 + |\beta|^2(1-r)}{2(2-r)},$$
$$P_{\mathrm{EAM}_{B_i}}(i=3,4) = \frac{|\beta|^2 + |\alpha|^2(1-r)}{2(2-r)}. \tag{27}$$

Similarly, by considering the $\varphi_{\mathrm{opt}}^{\mathrm{QGTP-EAM}}$ in equation (25), the total teleportation success probability of QGTP-EAM is described as

$$g_{\mathrm{tot}}^{\mathrm{QGTP-EAM}} = \sum_{i=1,2,3,4} g_{\mathrm{EAM}_{B_i}}^{f} = \frac{4}{4-2r}\cos^2\varphi_{\mathrm{opt}}^{\mathrm{QGTP-EAM}} = \frac{2(1-r)}{(2-r)^2}. \tag{28}$$

2.3. Performance comparison

We now proceed to numerically compare our proposed teleportation protocols and analyze their performance for different values of r. In the QGTP and QGTP-EAM, the aim is to maximize the average teleportation fidelity for each scheme by finding the optimum rotation gate angles and calculating the corresponding total teleportation success probability. A comparison of the results of three schemes [maximized QGTP (MQGTP), QGTP-EAM and the MR framework] is shown in figure 5. In figure 5(a), we plot the following: (1) the maximum average teleportation fidelity of the MQGTP in equation (14) by selecting the optimum rotation gate angle; (2) the average teleportation fidelity of the QGTP-EAM in

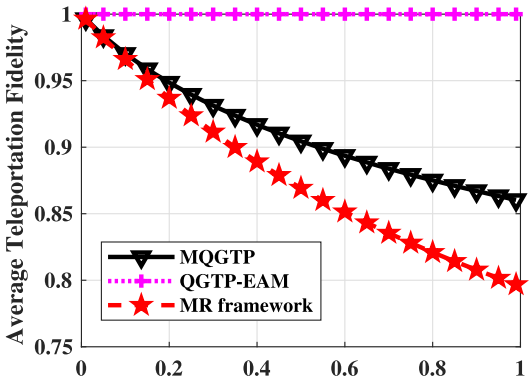

(a) Average teleportation fidelity vs. r.

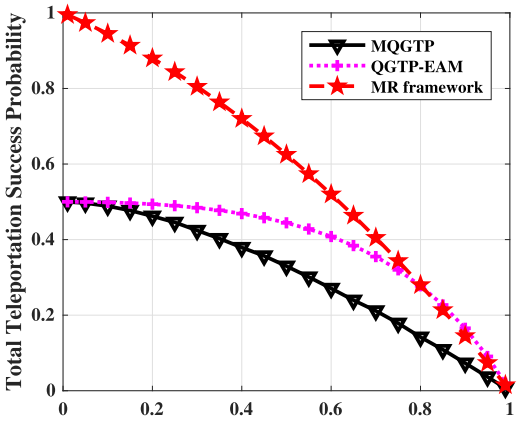

(b) Total teleportation success probability vs. r.

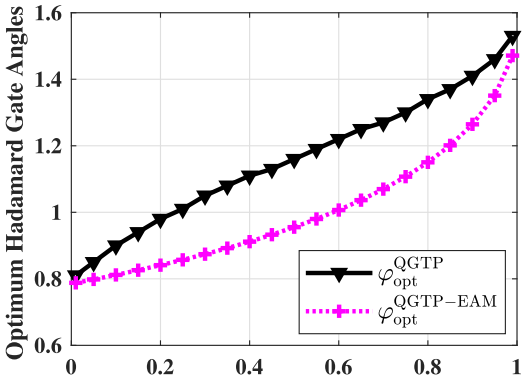

(c) Optimum rotation gate angles of QGTP and QGTP-EAM.

Figure 5. Comparison of the MQGTP, QGTP-EAM and MR frameworks.

equation (26) with the optimum rotation gate angle $\varphi_{opt}^{QGTP-EAM}$ in equation (25) to gain unit average teleportation fidelity; and (3) the average teleportation fidelity of the MR framework in equation (19), which uses weak measurement reversal. Moreover, figure 5(b) shows the result of comparing the following: (1) the corresponding total teleportation success probability of the MQGTP in equation (15); (2) the total teleportation success probability of the QGTP-EAM in equation (28); and (3) the total teleportation success probability of the MR framework in equation (20). Additionally, the optimum rotation gate angles of the two QGTPs are shown in figure 5(c).

As shown in figure 5(a), the two proposed teleportation protocols significantly improve the average teleportation fidelity compared with the MR framework. As we mentioned before, QGTP-EAM can obtain an average teleportation fidelity of unity independent of the magnitude of decoherence. The interesting point, according to figure 5(b), is that the total teleportation success probability of QGTP-EAM is higher than that of MQGTP for most values of r. Therefore, by adding EAM to QGTP, both the teleportation fidelity and the total teleportation success probability are improved. Moreover, as illustrated by figure 5(c), the optimum rotation gate angles in the MQGTP and QGTP-EAM are in the range of 0.8 to $\pi/2$. Therefore, assuming that EAM is available, it can be concluded that the QGTP-EAM is absolutely preferable.

3. Quantum gate-assisted entanglement distribution through amplitude damping channel

In the previous section, to overcome the effects of the decoherence channel we recovered the damped output state by modifying the teleportation process via a QGCU. In fact, as mentioned in section 1, the degradation of shared entangled states is the fundamental reason for the decrease in quantum teleportation fidelity. The proposed teleportation protocols are probabilistic, but in some cases its preferable to first distribute the entangled state between Alice and Bob and then implement a quantum teleportation protocol that works in a deterministic manner. The main motivation of this section is to use a QGCU in the entanglement distribution process and then employ a standard teleportation protocol. Hence, in this section, we consider applying QGCUs only in the entanglement distribution process. Before the decoherence channel,

Alice employs a QGCU on the second qubit of the entangled pair to transfer it to a state that is less vulnerable to the effects of the ADC; after the decoherence channel, Bob recovers his half of the entangled pair by applying another QGCU. After a successful entanglement distribution process, Alice and Bob proceed to the standard teleportation process. A schematic diagram of the proposed quantum gate-assisted entanglement distribution process (QGED) is depicted in figure 6.

Alice applies the QGCU explained in section 2.1 to the second qubit of the entangled pair that will be sent to Bob. As a result, after applying the QGCU and tracing out the ancilla qubit, the non-normalized density matrix of the entangled state is obtained as

$$\rho'_{ab} = \mathrm{Tr}_{A_1}[P_{A_1} C_1(\rho_{ab} \otimes \rho_{A_1}) C_1^\dagger P_{A_1}^\dagger] = \frac{1}{2}\begin{bmatrix} \cos^2\varphi_1 & 0 & 0 & \cos\varphi_1 \sin\varphi_1 \\ 0 & 0 & 0 & 0 \\ 0 & 0 & 0 & 0 \\ \cos\varphi_1 \sin\varphi_1 & 0 & 0 & \sin^2\varphi_1 \end{bmatrix}, \quad (29)$$

where $\rho_{A_1} = [\cos^2\varphi_1, \cos\varphi_1 \sin\varphi_1; \cos\varphi_1 \sin\varphi_1, \sin^2\varphi_1]$ is the density matrix of the ancilla qubit A_1 after it passes through a rotation gate with an angle φ_1, $C_1 = I_2 \otimes C$ is the CNOT gate with C in equation (7) and $P_{A_1} = I_2 \otimes I_2 \otimes |0\rangle\langle 0|$ is the measurement operator applied on A_1.

Afterwards, the second qubit of the entangled pair passes through an ADC defined by equation (A1), and the non-normalized density matrix of the shared entangled state evolves to

$$\rho_{ab}^{\mathrm{damp}'} = E_0 \rho'_{ab} E_0^\dagger + E_1 \rho'_{ab} E_1^\dagger = \frac{1}{2}\begin{bmatrix} \cos^2\varphi_1 & 0 & 0 & \cos\varphi_1 \sin\varphi_1 \sqrt{1-r} \\ 0 & 0 & 0 & 0 \\ 0 & 0 & r\sin^2\varphi_1 & 0 \\ \cos\varphi_1 \sin\varphi_1 \sqrt{1-r} & 0 & 0 & \sin^2\varphi_1 (1-r) \end{bmatrix}. \quad (30)$$

Following the receipt of the second qubit of the entangled pair at Bob's location, he applies the QGCU on his qubit. Hence, the normalized density matrix of the shared entanglement is obtained as

$$\rho_{ab}^{\mathrm{ED}} = \frac{\mathrm{Tr}_{A_2}[P_{A_2} C_1(\rho_{ab}^{\mathrm{damp}'} \otimes \rho_{A_2}) C_1^\dagger P_{A_2}^\dagger]}{\mathrm{Tr}\{\ \mathrm{Tr}_{A_2}[P_{A_2} C_1(\rho_{ab}^{\mathrm{damp}'} \otimes \rho_{A_2}) C_1^\dagger P_{A_2}^\dagger]\}} = \frac{1}{2g^{\mathrm{QGED}}}\begin{bmatrix} \cos^2\varphi_1 \cos^2\varphi_2 & 0 & 0 & \rho_{14} \\ 0 & 0 & 0 & 0 \\ 0 & 0 & r\cos^2\varphi_2 \sin^2\varphi_1 & 0 \\ \rho_{41} & 0 & 0 & \sin^2\varphi_1 \sin^2\varphi_2 (1-r) \end{bmatrix}, \quad (31)$$

where $\rho_{14} = \rho_{41} = \cos\varphi_1 \cos\varphi_2 \sin\varphi_1 \sin\varphi_2 \sqrt{1-r}$ and $\rho_{A_2} = [\cos^2\varphi_2, \cos\varphi_2 \sin\varphi_2; \cos\varphi_2 \sin\varphi_2, \sin^2\varphi_2]$ is the density matrix of the ancilla qubit A_2 after it passes through a rotation gate with an angle φ_2, $P_{A_2} = P_{A_1}$ is the measurement operator applied on A_2 and g^{QGED} is the success probability of QGED calculated as

$$g^{\mathrm{QGED}} = \mathrm{Tr}\{\ \mathrm{Tr}_{A_2}[P_{A_2} C_1(\rho_{ab}^{\mathrm{damp}'} \otimes \rho_{A_2}) C_1^\dagger P_{A_2}^\dagger]\} = \frac{1}{2}[\sin^2\varphi_1 (1-r)(2\sin^2\varphi_2 - 1) + \cos^2\varphi_2]. \quad (32)$$

This completes the QGED process. After successful entanglement distribution, Alice and Bob proceed to the standard teleportation process by considering the shared entangled state in equation (31). It is worth noting that the probability of gaining the measurement outcome corresponding to the measurement operators B_i is different from the case presented previously because of QGED. In this case, these probabilities are calculated as

$$\begin{aligned} P_{B_i}^{\mathrm{ED}}(i = 1, 2) &= \mathrm{Tr}[B_i(\rho_{\mathrm{in}} \otimes \rho_{ab}^{\mathrm{ED}}) B_i^\dagger] \\ &= \frac{|\alpha|^2(\cos^2\varphi_1 - \sin^2\varphi_2) + |\beta|^2 r \sin^2\varphi_1 (1 - 2\sin^2\varphi_2) + \sin^2\varphi_1 \sin^2\varphi_2}{2\sin^2\varphi_1 (1-r)(2\sin^2\varphi_2 - 1) + 2\cos^2\varphi_2}, \\ P_{B_i}^{\mathrm{ED}}(i = 3, 4) &= \mathrm{Tr}[B_i(\rho_{\mathrm{in}} \otimes \rho_{ab}^{\mathrm{ED}}) B_i^\dagger] \\ &= \frac{|\beta|^2(\cos^2\varphi_1 - \sin^2\varphi_2) + |\alpha|^2 r \sin^2\varphi_1 (1 - 2\sin^2\varphi_2) + \sin^2\varphi_1 \sin^2\varphi_2}{2\sin^2\varphi_1 (1-r)(2\sin^2\varphi_2 - 1) + 2\cos^2\varphi_2}. \end{aligned} \quad (33)$$

Since we used teleportation fidelity in the previous section to evaluate the performance of the proposed protocols, here we also investigate the average teleportation fidelity of the standard teleportation protocol by considering the shared entangled state from the QGED strategy in equation (31).

Therefore, after a successful QGED process, the output state received by Bob is described as

$$\rho_{B_i}^{f'}(i=1,2)=\begin{bmatrix}\frac{|\alpha|^2\cos^2\varphi_1\cos^2\varphi_2+|\beta|^2 r\cos^2\varphi_2\sin^2\varphi_1}{2\sin^2\varphi_1(1-r)(2\sin^2\varphi_2-1)+2\cos^2\varphi_2} & \frac{\alpha\beta^*\cos\varphi_1\cos\varphi_2\sin\varphi_1\sin\varphi_2\sqrt{1-r}}{2\sin^2\varphi_1(1-r)(2\sin^2\varphi_2-1)+2\cos^2\varphi_2}\\ \frac{\alpha^*\beta\cos\varphi_1\cos\varphi_2\sin\varphi_1\sin\varphi_2\sqrt{1-r}}{2\sin^2\varphi_1(1-r)(2\sin^2\varphi_2-1)+2\cos^2\varphi_2} & \frac{|\beta|^2\sin^2\varphi_1\sin^2\varphi_2(1-r)}{2\sin^2\varphi_1(1-r)(2\sin^2\varphi_2-1)+2\cos^2\varphi_2}\end{bmatrix},$$

$$\rho_{B_i}^{f'}(i=3,4)=\begin{bmatrix}\frac{|\alpha|^2\sin^2\varphi_1\sin^2\varphi_2(1-r)}{2\sin^2\varphi_1(1-r)(2\sin^2\varphi_2-1)+2\cos^2\varphi_2} & \frac{\alpha\beta^*\cos\varphi_1\cos\varphi_2\sin\varphi_1\sin\varphi_2\sqrt{1-r}}{2\sin^2\varphi_1(1-r)(2\sin^2\varphi_2-1)+2\cos^2\varphi_2}\\ \frac{\alpha^*\beta\cos\varphi_1\cos\varphi_2\sin\varphi_1\sin\varphi_2\sqrt{1-r}}{2\sin^2\varphi_1(1-r)(2\sin^2\varphi_2-1)+2\cos^2\varphi_2} & \frac{|\beta|^2\cos^2\varphi_1\cos^2\varphi_2+|\alpha|^2 r\cos^2\varphi_2\sin^2\varphi_1}{2\sin^2\varphi_1(1-r)(2\sin^2\varphi_2-1)+2\cos^2\varphi_2}\end{bmatrix}. \tag{34}$$

Thus, the teleportation fidelity between the input state in equation (1) and the final state received by Bob in equation (34) is calculated as

$$\begin{aligned}\mathrm{fid}_{\mathrm{ED}_i}(i=1,2)&=\langle\psi_{\mathrm{in}}|\rho_{B_i}^{f'}|\psi_{\mathrm{in}}\rangle\\&=\frac{|\beta|^4(1-r)(1-\cos^2\varphi_1-\cos^2\varphi_2+\cos^2\varphi_1\cos^2\varphi_2)+|\alpha|^4\cos^2\varphi_1\cos^2\varphi_2}{|\beta|^2\cos^2\varphi_2\sin^2\varphi_1+|\alpha|^2\cos^2\varphi_1\cos^2\varphi_2-|\beta|^2\sin^2\varphi_1(1-r)(1-2\cos^2\varphi_2)}\\&+\frac{|\alpha|^2|\beta|^2 r\cos^2\varphi_2\sin^2\varphi_1+2|\alpha|^2|\beta|^2\cos\varphi_1\cos\varphi_2\sin\varphi_1\sin\varphi_2\sqrt{1-r}}{|\beta|^2\cos^2\varphi_2\sin^2\varphi_1+|\alpha|^2\cos^2\varphi_1\cos^2\varphi_2-|\beta|^2\sin^2\varphi_1(1-r)(1-2\cos^2\varphi_2)},\\ \mathrm{fid}_{\mathrm{ED}_i}(i=3,4)&=\langle\psi_{\mathrm{in}}|\rho_{B_i}^{f'}|\psi_{\mathrm{in}}\rangle\\&=\frac{|\alpha|^4(1-r)(1-\cos^2\varphi_1-\cos^2\varphi_2+\cos^2\varphi_1\cos^2\varphi_2)+|\beta|^4\cos^2\varphi_1\cos^2\varphi_2}{|\alpha|^2\cos^2\varphi_2\sin^2\varphi_1+|\beta|^2\cos^2\varphi_1\cos^2\varphi_2-|\alpha|^2\sin^2\varphi_1(1-r)(1-2\cos^2\varphi_2)}\\&+\frac{|\alpha|^2|\beta|^2 r\cos^2\varphi_2\sin^2\varphi_1+2|\alpha|^2|\beta|^2\cos\varphi_1\cos\varphi_2\sin\varphi_1\sin\varphi_2\sqrt{1-r}}{|\alpha|^2\cos^2\varphi_2\sin^2\varphi_1+|\beta|^2\cos^2\varphi_1\cos^2\varphi_2-|\alpha|^2\sin^2\varphi_1(1-r)(1-2\cos^2\varphi_2)}.\end{aligned} \tag{35}$$

Hence, the average teleportation fidelity of the standard teleportation protocol with QGED over all possible input states is

$$\mathrm{Fid}_{\mathrm{av}}^{\mathrm{QGED}}=\int d\rho(P_{B_i}^{\mathrm{ED}}\mathrm{fid}_{\mathrm{ED}_i}). \tag{36}$$

For different values of r, each set of rotation gate angles (φ_1, φ_2) uniquely derives its corresponding entanglement distribution success probability and average teleportation fidelity, symbolized by a point (Fid_{av}^{QGED}—g^{QGED}). In figure 7, the rotation gate angles (φ_1, φ_2) are separately collected over all real numbers in the range $0\leqslant\varphi_1,\ \varphi_2\leqslant\pi/2$, and phase diagrams of corresponding average teleportation fidelity and entanglement distribution success probability (Fid_{av}^{QGED}—g^{QGED}) for selected values of $r=0.5$ and 0.8 are plotted. Each blue dot represents the (Fid_{av}^{QGED}—g^{QGED}) of a selected rotation gate angle set (φ_1, φ_2). The red line represents the average teleportation fidelity of the MR framework, the black line represents the maximized average teleportation fidelity of the QGTP and the green line is the average teleportation fidelity of the STNP. It should be stressed that the success probability in figure 7 corresponds to the entanglement distribution process rather than the teleportation process. In other words, once the entangled qubits have been successfully distributed between Alice and Bob, unit total teleportation success probability is always achieved by implementing the standard teleportation protocol.

In figure 7, for a given average teleportation fidelity (entanglement distribution success probability) the point (Fid_{av}^{QGED}—g^{QGED}) where the entanglement distribution success probability (average teleportation fidelity) is maximized is dispersed on the boundary line of the phase diagram. As figure 7 depicts, by selecting proper rotation gate angles (φ_1, φ_2), the QGED can improve the average teleportation fidelity compared with the QGTP and the MR framework. It is also possible to obtain an average teleportation fidelity of unity at the price of low success probability in the entanglement distribution process.

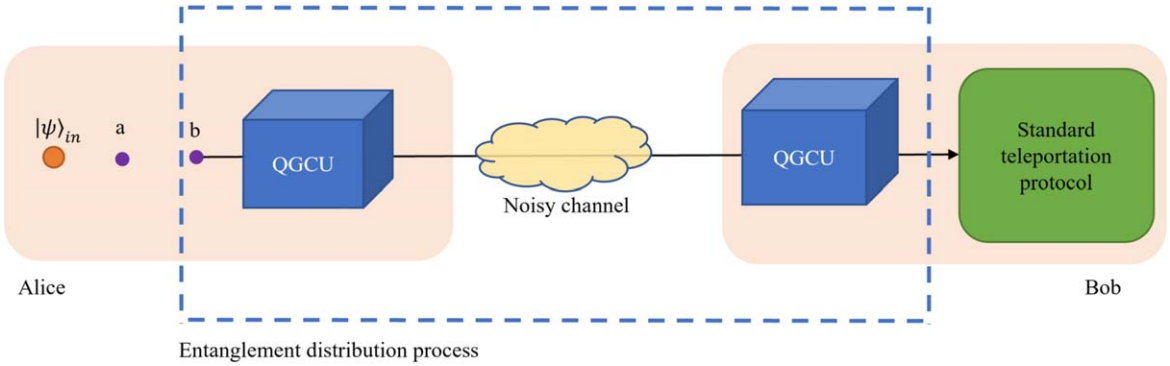

Figure 6. Schematic diagram of the quantum gate-assisted entanglement distribution process.

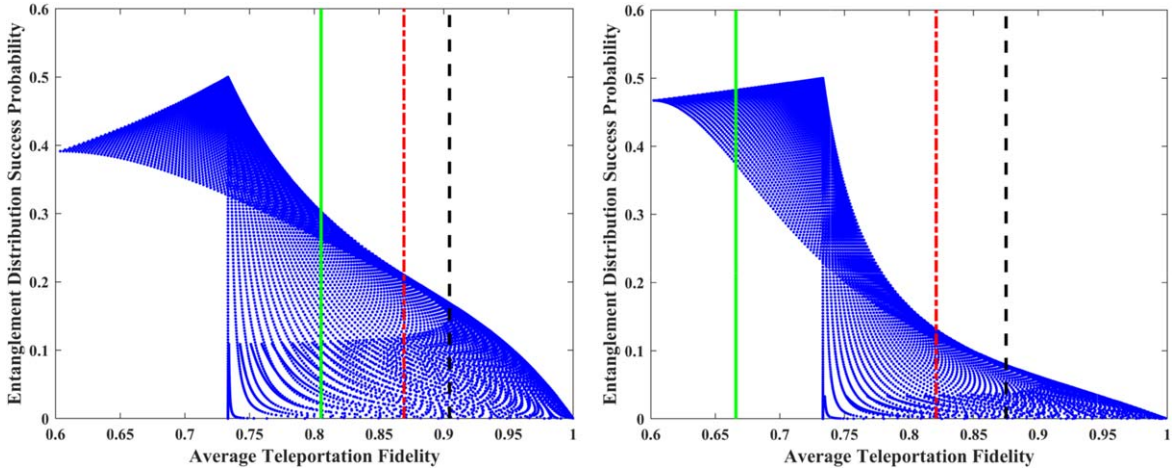

Figure 7. Phase diagram of ($\mathrm{Fid}_{av}^{\mathrm{QGED}}$—$g^{\mathrm{QGED}}$). Each blue dot represents the value of (Fid_{av}^{QGED}—g^{QGED}) for a selected set of rotation gate angles (φ_1, φ_2), collected over all real numbers within the range $0 \leqslant \varphi_1, \varphi_2 \leqslant \pi/2$. The solid green line represents the average teleportation fidelity of the STNP, the dash-dotted red line represents the average teleportation fidelity of the MR framework and the dashed black line represents the average teleportation fidelity of the MQGTP.

4. Conclusion

In this paper, we improved the fidelity of teleportation through noisy channels by utilizing a designed quantum gate control unit (QGCU). We proposed teleportation protocols and an entanglement distribution scheme via rotation and CNOT gates to teleport an unknown state through noisy channels with high fidelity. The proposed teleportation protocol applies a QGCU in the last step of teleportation to negate the effects of the noisy channel. The optimum rotation gate angles for maximizing the average teleportation fidelity were discovered by numerical simulations, and the corresponding total teleportation success probability was studied. Furthermore, unit average teleportation fidelity that is independent of the input state parameter and the magnitude of decoherence was achieved by integrating EAM with the quantum gate-assisted teleportation protocol. Moreover, to take advantage of a QGCU in a deterministic teleportation protocol, we considered employing QGCUs only in the entanglement distribution process followed by the standard teleportation protocol. It was demonstrated that our proposed schemes could greatly improve the average teleportation fidelity compared with the weak measurement-based teleportation in [43] and standard teleportation with no protection. The possible implementation schemes of the QGCU are given in a linear optics system [46] and in a cavity QED system where the quantum states are stored in superconducting cavities [55].

Funding

This work was supported by the National Natural Science Foundation of China under grant no. 61973290 and Ministry of Science and Technology of P. R. China Program under the grant no. QN2022200007L.

Competing interests

The authors declare that they have no competing interests.

Authors' contributions

SH conceived the idea, designed and performed experiments, analyzed results and wrote the manuscript and the revised manuscript. JZ performed experiments, analyzed results and wrote the manuscript. SC supervised the project. All authors discussed the results and commented on the manuscript.

Appendix

Here we explain the detailed procedure of the standard teleportation protocol through an ADC.

Since only one qubit of the entangled pair passes through the noisy channel, the applied Kraus operators for the entangled pair are

$$E_0 = I_2 \otimes e_0,\ E_1 = I_2 \otimes e_1. \tag{A1}$$

where e_i are the Kraus operators of the ADC in equation (3).

By considering the maximally entangled state prepared by Alice in equation (2), the non-normalized shared entangled state after passing through the ADC at Bob's end is described as

$$\begin{aligned}\rho_{ab}^{e} &= E_0\rho_{ab}E_0^{\dagger} + E_1\rho_{ab}E_1^{\dagger}\\ &= \frac{1}{2}\begin{bmatrix} 1 & 0 & 0 & \sqrt{1-r} \\ 0 & 0 & 0 & 0 \\ 0 & 0 & r & 0 \\ \sqrt{1-r} & 0 & 0 & 1-r \end{bmatrix},\end{aligned} \tag{A2}$$

where $\rho_{ab} = |\psi\rangle_{abab}\langle\psi|$ is the density matrix of the input state $|\psi\rangle_{ab}$ in equation (1).

To start the teleportation process, Alice interacts the input qubit in equation (1) with her half of the entangled pair. Thus, the combined system consisting of ρ_{in} and ρ_{ab}^{e} is

$$\rho_{\text{com}} = \rho_{\text{in}} \otimes \rho_{ab}^{e}. \tag{A3}$$

Alice makes a joint Bell state measurement on her two qubits (the input state and her share of the protected entangle state) with measurement operators $B_i = |b_i\rangle\langle b_i| \otimes I_2$, where $b_i (i = 1, 2, 3, 4)$ are defined as

$$\begin{aligned}|b_1\rangle &= \frac{1}{\sqrt{2}}(|00\rangle + |11\rangle),\ |b_2\rangle = \frac{1}{\sqrt{2}}(|00\rangle - |11\rangle),\\ |b_3\rangle &= \frac{1}{\sqrt{2}}(|01\rangle + |10\rangle),\ |b_4\rangle = \frac{1}{\sqrt{2}}(|01\rangle - |10\rangle).\end{aligned} \tag{A4}$$

After applying the joint measurement, Alice sends the result of the measurement to Bob through a classical channel. Thus, Bob knows that his state is now described as

$$\rho_{B_i} = \text{Tr}_{\bar{1}2}(B_i\rho_{\text{com}}B_i^{\dagger}), \tag{A5}$$

where $\text{Tr}_{\bar{1}2}(\bullet)$ denotes the partial trace on qubits 1 and 2 (those with Alice) and $P_{B_i} = \text{Tr}(B_i\rho_{\text{com}}B_i^{\dagger})$ is the probability of gaining the measurement outcome corresponding to the measurement operator B_i as

$$P_{B_i}(i = 1, 2, 3, 4) = \frac{1}{4}. \tag{A6}$$

According to the result of Alice's measurement, for each measurement operator B_i, Bob applies corresponding unitary operations on his qubit as

$$U_1 = I_2,\ U_2 = \sigma_z,\ U_3 = \sigma_x,\ U_4 = \sigma_x\sigma_z. \tag{A7}$$

Hence, Bob's non-normalized states, corresponding to Alice's measurement result B_i after applying unitary operations in equation (A7), are described as

$$\begin{aligned}\rho_{B_i}^{U_i}(i = 1, 2) &= U_i\rho_{B_i}U_i^{\dagger}\\ &= \frac{1}{4}\begin{bmatrix} |\alpha|^2 + |\beta|^2 r & \alpha\beta^*\sqrt{1-r} \\ \alpha^*\beta\sqrt{1-r} & |\beta|^2(1-r) \end{bmatrix},\\ \rho_{B_i}^{U_i}(i = 3, 4) &= U_i\rho_{B_i}U_i^{\dagger}\\ &= \frac{1}{4}\begin{bmatrix} |\alpha|^2(1-r) & \alpha\beta^*\sqrt{1-r} \\ \alpha^*\beta\sqrt{1-r} & |\beta|^2 + |\alpha|^2 r \end{bmatrix},\end{aligned} \tag{A8}$$

where ρ_{B_i} are Bob's reduced density matrices in equation (A5) and U_i are the corresponding unitary operations given in equation (A7).

References

[1] Pirandola S, Eisert J, Weedbrook C, Furusawa A and Braunstein S L 2015 Advances in quantum teleportation *Nat Photonics.* **9** 641–52

[2] Song D, He C, Cao Z and Chai G 2018 Quantum teleportation of multiple qubits based on quantum Fourier transform *IEEE Commun. Lett.* **22** 2427–30

[3] Xu R Q, Zhou R G, Li Y C, Jiang S X and Ian H 2022 Enhancing robustness of noisy qutrit teleportation with Markovian memory *EPJ. Quantum. Technol.* **9** 4

[4] Jahanbakhsh F and Tavassoly M K 2023 Teleportation of unknown states of a qubit and a single-mode field in strong coupling regime without Bell-state measurement *Commun. Theor. Phys.* **75** 025103

[5] He M-Y, Ma S-Y and Kang K-P 2021 A universal protocol for bidirectional controlled teleportation with network coding *Commun. Theor. Phys.* **73** 105104

[6] Schaetz T *et al* 2004 Quantum dense coding with atomic qubits *Phys. Rev. Lett.* **93** 040505

[7] Guo Y, Liu B H, Li C F and Guo G C 2019 Advances in quantum dense coding *Adv. Quantum. Technol.* **2** 1900011

[8] Chen Y, Liu S, Lou Y and Jing J 2021 Orbital angular momentum multiplexed quantum dense coding *Phys. Rev. Lett.* **127** 093601

[9] Bell B A *et al* 2014 Experimental demonstration of graph-state quantum secret sharing *Nat. Commun.* **5** 5480

[10] Qin H, Tang W K S and Tso R 2020 Hierarchical quantum secret sharing based on special high-dimensional entangled state. IEEE .J. Sel .Top *Quantum .Electron.* **26** 6600106

[11] Senthoor K and Sarvepalli P K 2022 Theory of communication efficient quantum secret sharing *IEEE Trans. Inf. Theory.* **68** 3164–86

[12] Pereira D, Almeida M, Facão M, Pinto A N and Silva N A 2021 Impact of receiver imbalances on the security of continuous variables quantum key distribution *EPJ . Quantum .Technol.* **8** 22

[13] Amer O, Garg V and Krawec W O 2021 An introduction to practical quantum key distribution *IEEE Aerosp Electron Syst. Mag.* **36** 30–55

[14] Cao Y, Zhao Y, Wang Q, Zhang J, Ng S X and Hanzo L 2022 The evolution of quantum key distribution networks: on the road to the qinternet *IEEE Commun. Surv. Tut.* **24** 839–94

[15] Nielsen M A and Chuang I L 2011 *Quantum. Computation and Quantum Information* (Cambridge: Cambridge University Press)

[16] Cacciapuoti A S, Caleffi M, Tafuri F, Cataliotti F S, Gherardini S and Bianchi G 2020 Quantum internet: networking challenges in distributed quantum computing *IEEE Netw.* **34** 137–43

[17] Rota M B, Basset F B, Tedeschi D and Trotta R 2020 Entanglement teleportation with photons from quantum dots: toward a solid-state based quantum network *IEEE J. Sel. Top Quantum. Electron.* **26** 6400416

[18] Ying M and Feng Y 2009 An algebraic language for distributed quantum computing *IEEE Trans. Comput.* **58** 728–43

[19] Lan J H, Lu X J and Kuang S 2022 Multi-hop remote single qubit state preparation based on arbitrary Bell states *Int. J. Theor. Phys.* **61** 240

[20] Cuomo D, Caleffi M and Cacciapuoti A S 2020 Towards a distributed quantum computing ecosystem *IET Quantum Commun.* **1** 3–8

[21] Bennett C H, Brassard G, Crépeau C, Jozsa R, Peres A and Wootters W K 1993 Teleporting an unknown quantum state via dual classical and Einstein–Podolsky–Rosen channels *Phys. Rev. Lett.* **70** 1895–9

[22] Karlsson A and Bourennane M 1998 Quantum teleportation using three-particle entanglement *Phys. Rev.* A **58** 4394–400

[23] Agrawal P and Pati A 2006 Perfect teleportation and superdense coding with W states *Phys. Rev.* A **74** 062320

[24] Breuer H P and Petruccione F 2007 *The Theory of Open Quantum. Systems* (Oxford: Oxford University Press)

[25] Cong S 2014 *Control of Quantum Systems: Theory and Methods* (New York: Wiley)

[26] Chandra D, Cacciapuoti A S, Caleffi M and Hanzo L 2022 Direct quantum communications in the presence of realistic noisy entanglement *IEEE Trans. Commun.* **70** 469–84

[27] Cacciapuoti A S, Caleffi M, Van Meter R and Hanzo L 2020 When entanglement meets classical communications: quantum teleportation for the quantum internet *IEEE Trans Commun.* **68** 3808–33

[28] Darmawan A S and Poulin D 2017 Tensor-network simulations of the surface code under realistic noise *Phys. Rev. Lett.* **119** 040502

[29] Yan H *et al* 2022 Entanglement purification and protection in a superconducting quantum network *Phys .Rev. Lett.* **128** 080504

[30] Li W C, Xiao Y, Han X H, Fan X, Hei X B and Gu Y J 2023 Dynamics of multipartite quantum steering for different types of decoherence channels *Sci. Rep.* **13** 3798

[31] Hu Z, Xia R and Kais S 2020 A quantum algorithm for evolving open quantum dynamics on quantum computing devices *Sci. Rep.* **10** 3301

[32] Kim Y S, Lee J C, Kwon O and Kim Y H 2012 Protecting entanglement from decoherence using weak measurement and quantum measurement reversal *Nat Phys.* **8** 117–20

[33] Kim Y S, Cho Y W, Ra Y S and Kim Y H 2009 Reversing the weak quantum measurement for a photonic qubit *Opt. Express.* **17** 11978–85

[34] Singh U, Mishra U and Dhar H S 2014 Enhancing robustness of multiparty quantum correlations using weak measurement *Ann. Phys. (N Y).* **350** 50–68

[35] Wang C *et al* 2014 Feed-forward control for quantum state protection against decoherence *Phys. Rev.*A **89** 032303

[36] Guo L S *et al* 2015 Discriminating two nonorthogonal states against a noise channel by feed-forward control *Phys. Rev.* A **91** 022321

[37] Li Y L, Zu C J and Wei D M 2019 Enhance quantum teleportation under correlated amplitude damping decoherence by weak measurement and quantum measurement reversal *Quantum. Inf. Process.* **18** 2

[38] Harraz S, Cong S and Nieto J J 2022 Enhancing quantum teleportation fidelity under decoherence via weak measurement with flips *EPJ. Quantum. Technol.* **9** 15

[39] Harraz S, Cong S and Nieto J J 2021 Protected quantum teleportation through noisy channel by weak measurement and environment-assisted measurement *IEEE Commun. Lett.* **26** 528–31

[40] Zhao X, Hedemann S R and Yu T 2013 Restoration of a quantum state in a dephasing channel via environment-assisted error correction *Phys. Rev.* A **88** 022321

[41] Azuma K, Tamaki K and Lo H K 2015 All-photonic quantum repeaters *Nat Commun.* **6** 6787

[42] Harraz S, Zhang J Y and Cong S 2023 High-fidelity quantum teleportation through noisy channels via weak measurement and environment-assisted measurement *Results Phys.* **55** 107164

[43] Im D *et al* 2021 Optimal teleportation via noisy quantum channels without additional qubit resources *Npj. Quantum. Inf.* **7** 86

[44] Lee S W, Im D G, Kim Y H, Nha H and Kim M S 2021 Quantum teleportation is a reversal of quantum measurement *Phys. Rev. Res.* **3** 033119

[45] Al Amri M, Scully M O and Zubairy M S 2011 Reversing the weak measurement on a qubit *J .Phys. B: At. Mol. Opt. Phys.* **44** 165509

[46] Liao Z, Al-Amri M and Zubairy M S 2013 Protecting quantum entanglement from amplitude damping *J. Phys. B: At. Mol. Opt. Phys.* **46** 145501

[47] Esfahani S S, Liao Z and Zubairy M S 2016 Robust quantum state recovery from amplitude damping within a mixed states framework *J .Phys. B: At. Mol .Opt. Phys.* **49** 155501

[48] Zhao Z *et al* 2005 Experimental demonstration of a nondestructive controlled-NOT quantum gate for two independent photon qubits *Phys. Rev. Lett.* **94** 30501

[49] Lin Q and Li J 2009 Quantum control gates with weak cross-Kerr nonlinearity *Phys. Rev.* A **79** 022301

[50] Xiu X-M, Dong L, Gao Y-J and Yi X X 2012 Nearly deterministic controlled-not gate with weak cross-Kerr nonlinearities *Quantum. Inf. Comput.* **12** 159–70

[51] Bowdrey M D, Oi D K L, Short A J, Banaszek K and Jones J A 2002 Fidelity of single qubit maps *Phys. Lett.* A **294** 258–60

[52] Gregoratti M and Werner R F 2003 Quantum lost and found *J Mod. Opt.* **50** 915–33

[53] Wang K, Zhao X and Yu T 2014 Environment-assisted quantum state restoration via weak measurements *Phys. Rev.* A **89** 042320

[54] Li Y L, Sun F, Yang J and Xiao X 2021 Enhancing the teleportation of quantum Fisher information by weak measurement and environment-assisted measurement *Quantum .Inf. Process.* **20** 55

[55] Zeng X, Ge G Q and Zubairy M S 2019 Quantum state protection in finite-temperature environment via quantum gates *Opt. Express.* **27** 25789–801